Printed Microwave Couplers with Thermal Isolation

Robert A. Brown, Peyman Ensaf, Todd Marshall, Melinda Piket-May, Branko Popović, and Zoya Popović

Department of Electrical and Computer Engineering
University of Colorado
Boulder, CO 80309

Abstract—

This paper discusses design principles and measurements for three printed microwave couplers designed for thermal isolation. These couplers are intended to minimize heat leakage when used as connectors to a cryostat, thereby maintaining the low temperature for a longer period of time. The first coupler is designed for L-band operation and exhibits a 10 dB return loss and 2 dB insertion loss. The second design operates in the cellular band with a maximum return loss of 28 dB and insertion loss less than 0.5 dB. Simple thermal modeling suggests significant improvements over standard coaxial connections. The third coupler is designed for X-band with a 15.6 dB return loss and a measured insertion loss of a few tenths of a dB at 10 GHz.

I. Introduction

SUPERCONDUCTING technology holds promise for a variety of microwave applications, for example very selective filter banks for cellular base stations [1]. The transition from the super-cooled environment to the outside environment poses an interesting challenge, since it is desirable to maintain signal level and bandwidth while minimizing heat transfer between the two environments. Because electrical conductors generally are excellent heat conductors, one approach to reducing the amount of thermal transfer is to break any continuous metal path between the cryostat and its outside environment. This approach has been demonstrated by Davidovitz [2], whose structure consists of two waveguide sections separated by a small air gap and exhibits less than 0.5 dB insertion loss between 19 GHz and 24 GHz. However, since waveguide structures are large and expensive in the cellular, PCS, and X-bands, our goal is to investigate a solution to the thermal-isolation problem which utilizes printed microwave structures.

Two of the couplers presented here are envisioned as a pair of electrically small planar near-field antennas which utilize resonant coupling to achieve electrical transmission. Although the dielectric layer between the antennas allows heat conduction, the thermal resistance of the dielectric interface is much greater than that of a direct metal connection. The first of these geometries is shown in Figure 1 and consists of two spiral elements.

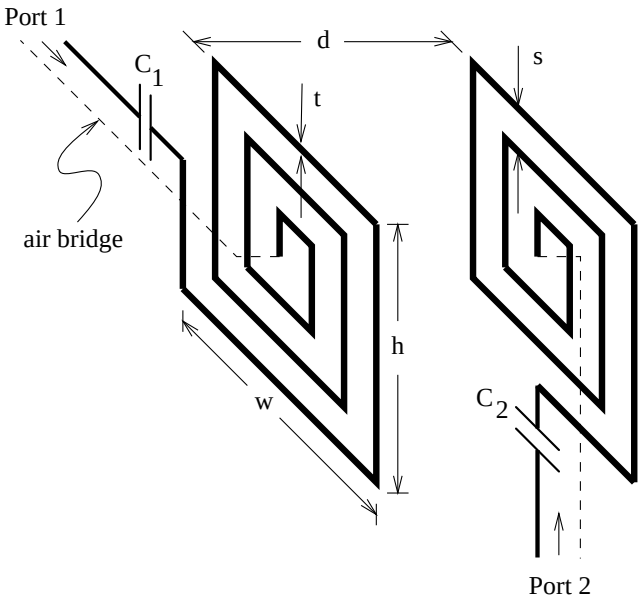

Fig. 1. The spiral coupler. The spirals are printed on opposite sides of a dielectric substrate ($\epsilon_r = 2.17$) with thickness $d = 0.5\,\text{mm}$. The dashed lines represent air bridges which are used to bring the centers of the spirals to ground potential. The lumped capacitors, C_1 and C_2, are used to tune the coupler's S_{11} and S_{12} parameters. The design presented here has $h = 12\,\text{mm}$, $w = 14\,\text{mm}$, $s = 0.9\,\text{mm}$, and $t = 1.1\,\text{mm}$. Ports 1 and 2 are $50\,\Omega$ microstrip lines.

The second coupler (Figure 2) is a pair of fork-shaped elements. The third coupler shown in Figure 3 is not resonant, but is a pair of capacitively coupled coplanar waveguides.

0-7803-4603-6/97/$5.00 (c) IEEE

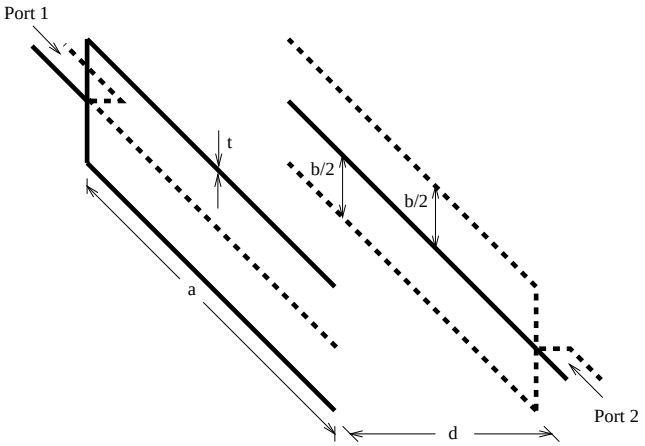

Fig. 2. The fork coupler. Each of the two forks is printed on a thin dielectric substrate (thickness = 0.5 mm) and then separated by a variable distance d. Two branches of each fork are printed on one side of the substrate, while the third branch is printed on the opposite side. For the design presented here, $a = 8$ cm, $b = 2$ cm, and $t = 2$ mm.

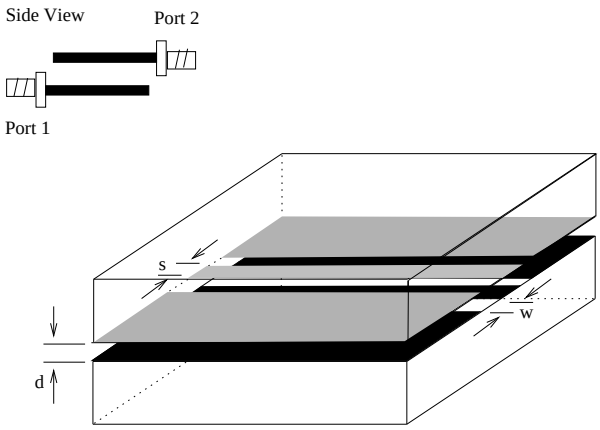

Fig. 3. The CPW coupler. The CPW is printed on a 1.27 mm thick substrate with $\epsilon_r = 10.5$. The separation distance is $d \approx 150\ \mu$m. Also, $s = 2.2$ mm and $w = 0.784$ mm.

II. The Electrical Properties of the Spiral Coupler

The spiral coupler was first designed and analyzed using the numerical electromagnetic analysis program *WireZeus* [3]. *WireZeus* is based on an approximate full-wave solution to Hallen's integral equation, and is computationally efficient. The moment method uses entire-domain basis functions and an equivalent radius and coating for analyzing printed structures.

The spiral coupler uses two lumped capacitors, $C_1 = 1.5$ pF and $C_2 = 0.5$ pF, to tune out the self-inductance and to provide high return loss at each port. The spirals are fabricated back–to–back on a Duroid substrate having a dielectric constant of 2.17 and thickness of 0.5 mm. The branches of the spirals are $t = 1.1$ mm wide and the wire bridges are 1.5 mm above the planes of the spirals, with diameters of 0.3 mm.

The VSWR of the coupler is designed to be less than 1.2 in the PCS band. The radiation loss as predicted by *WireZeus* is approximately 0.1%. Measurements were performed on an HP8510B network analyzer using coaxial calibration, and Figure 4 shows these results. The

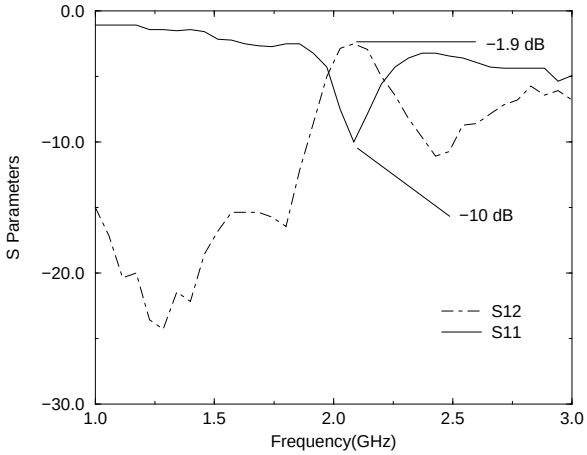

Fig. 4. Measured S_{11} and S_{12} for the spiral coupler. Coaxial calibration up to the microstrip feeds was used.

coupler has a 1.9 dB insertion loss at 2 GHz and a 3–dB bandwidth of 40 MHz. The discrepancies between numerical and measured results can be explained as follows: a) the feed lines are not modeled in the numerical design; b) *WireZeus* cannot accurately model segments that are much smaller than a wavelength (the equivalent radius approximation becomes inaccurate); c) the tuning capacitors have large tolerances, 50% for the 0.5 pF capacitor and the resonant nature of the coupler makes it sensitive to reactance variations; and d) the design is sensitive to the geometry of the wire bridge.

III. The Electrical Properties of the Fork Coupler

Figure 2 shows the fork-shaped design for the cellular band. The coupler consists of two thin planar substrates with printed metal traces. The coupler is connected at ports 1 and 2 via a short segment of microstrip line and a microstrip–coaxial transition.

The analysis and design of the coupler are completed using *WireZeus*. Two important design parameters are fork width and fork length, which control the input impedance and operating frequency, respectively. In-

0-7803-4603-6/97/$5.00 (c) IEEE

creasing the width of the forks ($b/2$ in Figure 2) increases the impedance looking into either port. The operating frequency is selected by satisfying $2a + (b/2) = \lambda_0/2$.

The coupler is fabricated on two separate Duroid substrates ($\epsilon_r = 2.17$, thickness=0.508 mm) and tested around 900 MHz. Figure 5 shows the measured results

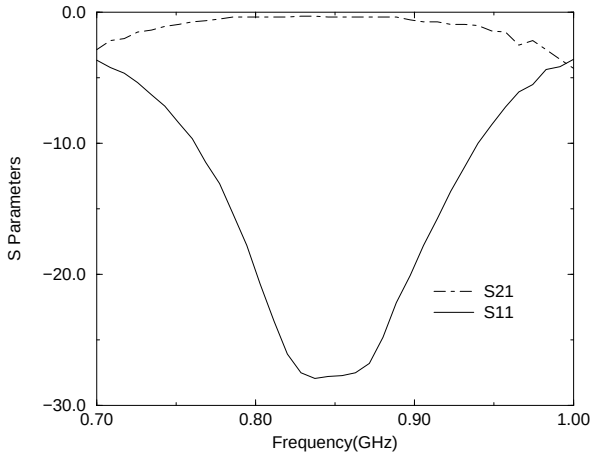

Fig. 5. The measured S-parameters of the fork coupler. The symmetry of the scattering parameters is evident and is a result of the geometrical symmetry of the coupler.

of this design with a coaxial calibration. The minimum return loss, 28.0 dB, is centered at 850 MHz and the coupler exhibits a 3–dB bandwidth of 60 MHz. The minumum insertion loss for this design is 0.5 dB.

IV. The Electrical Properties of the Coplanar Waveguide Coupler

Figure 3 shows the configuration of the coplanar waveguide (CPW) coupler. The two CPW lines are seperated by a thin gap, $d \approx 150\,\mu$m, filled with a dielectric. The dielectric gap provides a large thermal resistance and controls the capacitive coupling.

Figure 6 shows the measured results of this design with a CPW TRL calibration. The return loss at 10 GHz is 15.6 dB with an insertion loss of a few tenths of a dB within calibration error. The coupler exhibits a flat S_{21} from 9 GHz to 11 GHz.

V. Thermal Modeling

A simple case of conductive thermal modeling was performed using a finite element program, *Fluent* [4]. We chose a simple geometry common to all of the three presented couplers, as shown in Figure 7, and compared it to a single 1–mm wide metal through–line on top of

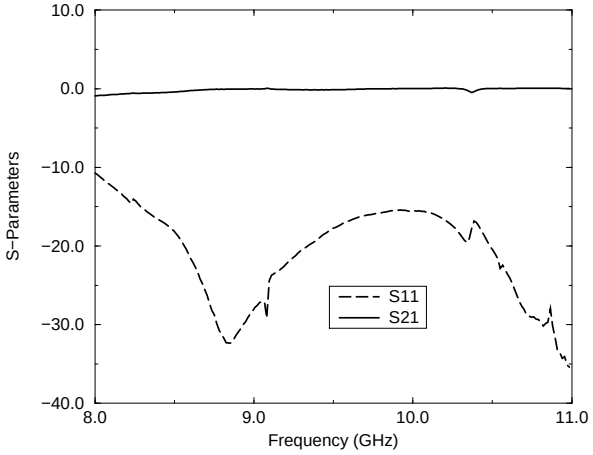

Fig. 6. The measured S-parameters of the CPW coupler using CPW TRL calibration. Within X-band, S_{21} is broadband with minimal loss.

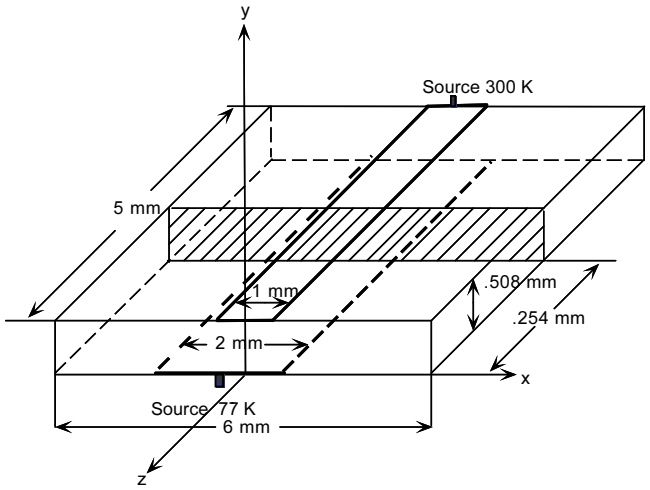

Fig. 7. The 77 K thermal load is placed at the origin on the bottom surface. The 300 K thermal load is placed at $z = 5$ mm and $y = 0.508$ mm on the top surface. This model was simulated using symmetry about the yz–plane.

the substrate. In the model shown in Figure 7, we have assumed adiabatic conditions and the thermal sources are single points where thermal loads of 300 K and 77 K are placed. The temperature profile at the upper and lower surface is modeled for the shaded cross section halfway between the two thermal sources. The profiles are shown in Figure 8 as compared to the single through–line, with a 78 K lower temperature in the middle of the line at $y = 0$ in the case of the double strip. This confirms that devices without a continuous metal connection improve thermal isolation. Thermal mea-

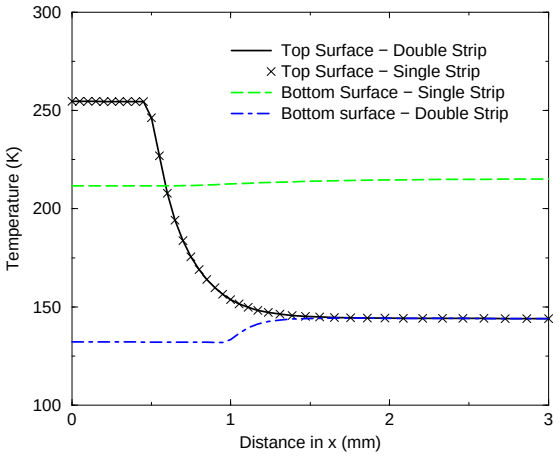

Fig. 8. A comparasion of the temperature profiles between a continous metal line (Single strip) and two continous metal lines separated by a dielectric (Double strip) is shown. The case of the double strip is illustrated in Figure 7 and the temperature profile corresponds to the shaded area.

surements of these devices in a cryostat environment are currently in progress.

Acknowledgments

This work was funded by Superconducting Core Technologies (SCT), Inc. (Golden, CO) through an Air Force STTR Phase II program. We thank Michael Ulsh in Mechanical Engineering at University of Colorado–Boulder for help with the thermal analysis, and Prof. Edward Kuester at University of Colorado–Boulder for many valuable discussions.

References

[1] Michael Cromar, *Private Communications*, SCT, Inc., Golden, CO.

[2] Marat Davidovitz, "A low-loss thermal isolator for waveguides and coaxial transmission lines," *IEEE Microwave and Guided Wave Letters*, vol. 6, no. 1, pp. 25–27, January 1996.

[3] B.D. Popović, *CAD of Wire Antennas and Related Radiating Structures*, Wiley, 1991.

[4] Fluent Incorporated, Centerra Resource Park, Lebanon, NH, *Fluent*, 1995.